

## On the importance of non-thermal far-field blooming in broad-area high-power laser diodes

Joachim Piprek<sup>1,a)</sup> and Z. M. Simon Li<sup>2</sup>

<sup>1</sup>NUSOD Institute LLC, P.O. Box 7204, Newark, Delaware 19714, USA

<sup>2</sup>Crosslight Software Inc., 121-3989 Henning Drive, Burnaby, British Columbia V5C 6P8, Canada

(Received 20 March 2013; accepted 25 May 2013; published online 5 June 2013)

High-power broad-area laser diodes often suffer from a widening of the slow-axis far-field with increasing current (lateral far-field blooming). This effect is commonly attributed to self-heating. Utilizing self-consistent electro-thermal-optical simulations, we analyze previous experimental investigations of 970 nm broad-area GaAs-based Fabry-Perot lasers and reproduce the blooming mechanism in good agreement with the measurements. The simulations reveal that a substantial part of the far field blooming is not caused by self-heating but by increasing carrier and gain non-uniformity in the quantum wells. © 2013 AIP Publishing LLC.

[<http://dx.doi.org/10.1063/1.4809835>]

High-power broad-area laser diodes typically exhibit a widening of the lateral far-field with increasing current which is detrimental, e.g., to applications that require the coupling of the laser beam into an optical fiber. This effect is often referred to as thermal far-field blooming, since self-heating is considered the main cause.<sup>1</sup> The lateral heat flow away from the active region causes a non-uniform temperature profile which creates a lateral refractive index gradient, a so-called thermal lens, that enhances the index guiding of laser modes. As a consequence, an increasing order of lateral modes is excited with rising current, which exhibit a wider far field. Using self-consistent electro-thermal-optical laser simulation, we here reproduce this behavior quantitatively and show that non-thermal mechanisms contribute substantially to the far-field blooming.

Numerical simulation is a valuable tool to study the complex interaction of electronic, thermal, and optical processes involved in the blooming process.<sup>2-5</sup> We employ a customized version of the LASTIP laser simulation software,<sup>6</sup> which allows for the self-consistent combination of multi-mode wave guiding, drift-diffusion of electrons and holes, heat generation, and heat flow in the transverse plane ( $x,y$ ). Lateral laser modes are calculated from the Helmholtz equation, including gain guiding and resulting in a different wavelength for each lateral mode. The modal far-fields are obtained from the Fourier transform of the modal near-field at the laser facet.<sup>7</sup> The optical power of each lateral mode is coupled directly with the drift-diffusion equations using the photon rate equations. The reason for the direct coupling is the strong dependence of the optical power on bias and local optical gain. The heat flow equations and lateral mode profile solvers are indirectly coupled and updated at every iteration step using results from a previously converged solution of the coupled drift-diffusion-optical-power equations. The indirect coupling is warranted since both the temperature and lateral mode profile (not the power itself) are slow functions of the bias. The heat power distribution is calculated from the local densities of current, carriers, and photons.

Joule heat, non-radiative recombination heat inside the quantum wells, and heat caused by modal absorption were identified as main heat sources.<sup>8</sup> Besides the laser chip, the simulation domain also includes the 250  $\mu\text{m}$  thick CuW submount (width = 650  $\mu\text{m}$ ) to accurately calculate the temperature profile  $T(x,y)$ . The local refractive index  $N(T,x,y)$  is obtained from the temperature distribution using published material parameters.<sup>9</sup> The average (modal) thermal index change is  $dN/dT = 3 \times 10^{-4}/\text{K}$ . The carrier-induced index change in the quantum wells is considered using an anti-guiding parameter of  $dN/dn = dN/dp = -0.5 \times 10^{-20} \text{ cm}^3$  ( $n$ ,  $p$ -density of electrons and holes, respectively). Model and parameters are the same as in our recent investigation of thermal blooming,<sup>8</sup> but we here reveal the importance of non-thermal effects by comparing and analyzing simulation results with and without self-heating.

Our analysis is based on the previous experimental characterization of a GaAs-based laser diode.<sup>1,10</sup> This Fabry-Perot laser features a compressively strained double quantum well (QW) InGaAs/GaAsP active region that is sandwiched between AlGaAs waveguide and cladding layers. The p-contact is 50  $\mu\text{m}$  wide and dry-etched trenches are located at 5  $\mu\text{m}$  distance on either side of the contact. The etch depth is about half the depth of the quantum wells and provides a built-in effective index step of  $17 \times 10^{-4}$ . The laser is mounted p-side down onto a CuW submount. The laser cavity is 1 mm long and the facet reflectivities are 5% and 95%. The relatively small size of this laser causes a large mode spacing as well as thermal lensing effects at relatively low current. The experimental investigation was restricted to currents up to 1.5 A, which corresponds to a relatively high current density of 3  $\text{kA}/\text{cm}^2$ .

The simulated light-current and current-voltage characteristics are in excellent agreement with the measurements (Fig. 1). The key process causing thermal blooming is the temperature rise in the waveguide region, which not only depends on the heat generation but also on the heat dissipation. The total thermal resistance  $R_{\text{th}}$  of the laser is controlled by the thermal conductivity of each semiconductor layer as well as by the quality of mounting and heat sinking. Thus,

<sup>a)</sup>piprek@nusod.org

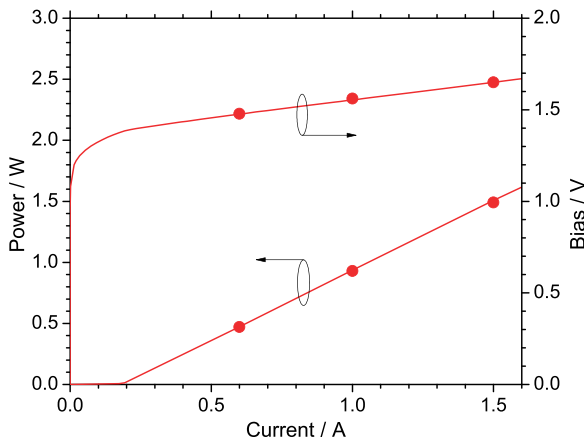


FIG. 1. Light-current (left) and bias-current (right) characteristics: comparison of simulation (lines) and measurement (symbols).

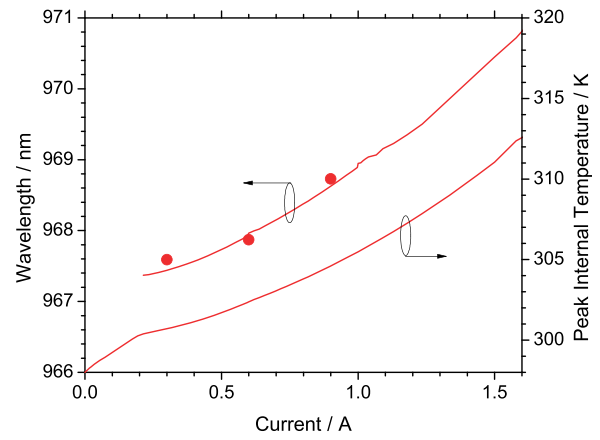


FIG. 2. Lasing wavelength vs. current (left) and maximum internal temperature vs. current (right). The symbols show the measured emission wavelength (measurements above 1 A are not available for this device).

the actual value of  $R_{th}$  is hard to predict theoretically and we therefore fit the measured wavelength shift (Fig. 2) by varying the unknown external thermal resistance outside the simulated region, applying a so-called mixed thermal boundary condition to the bottom of the CuW submount.<sup>11</sup> The maximum internal temperature is also plotted in Fig. 2, the temperature increase of 13 K at 1.5 A is in perfect agreement with the previous analysis of this laser.<sup>1</sup>

For illustration of the thermal blooming mechanism, Fig. 3 plots relevant lateral profiles calculated within the top quantum well at the experimental reference currents of 0.6 A, 1 A, and 1.5 A. The heat power density peaks near the p-contact edge at  $x = 25 \mu\text{m}$  (Fig. 3(a)), partially due to current crowding. The lateral temperature profile in Fig. 3(b)

remains relatively flat, it drops only by 1.4 K between the symmetry plane in the center ( $x = 0$ ) and the trench position at  $x = 30 \mu\text{m}$  (1.5 A). This lateral temperature drop is about one quarter of what was previously assumed.<sup>1</sup> The temperature gradient results in the formation of a thermal lens (Fig. 3(c)), the thermal index change is about  $30 \times 10^{-4}$  in the center of the laser, but the index drop between center and trench is only  $3.8 \times 10^{-4}$ , much smaller than the built-in effective index step of  $17 \times 10^{-4}$ . The carrier-induced effective index drop in Fig. 3(c) is about  $-3 \times 10^{-4}$  between center and trench and it slightly narrows the thermal lens. The resulting width of the simulated near field remains almost constant (Fig. 3(d)) and it is in good agreement with the measured full  $1/e^2$  width of the near field ( $52 \mu\text{m}$ ).<sup>10</sup>

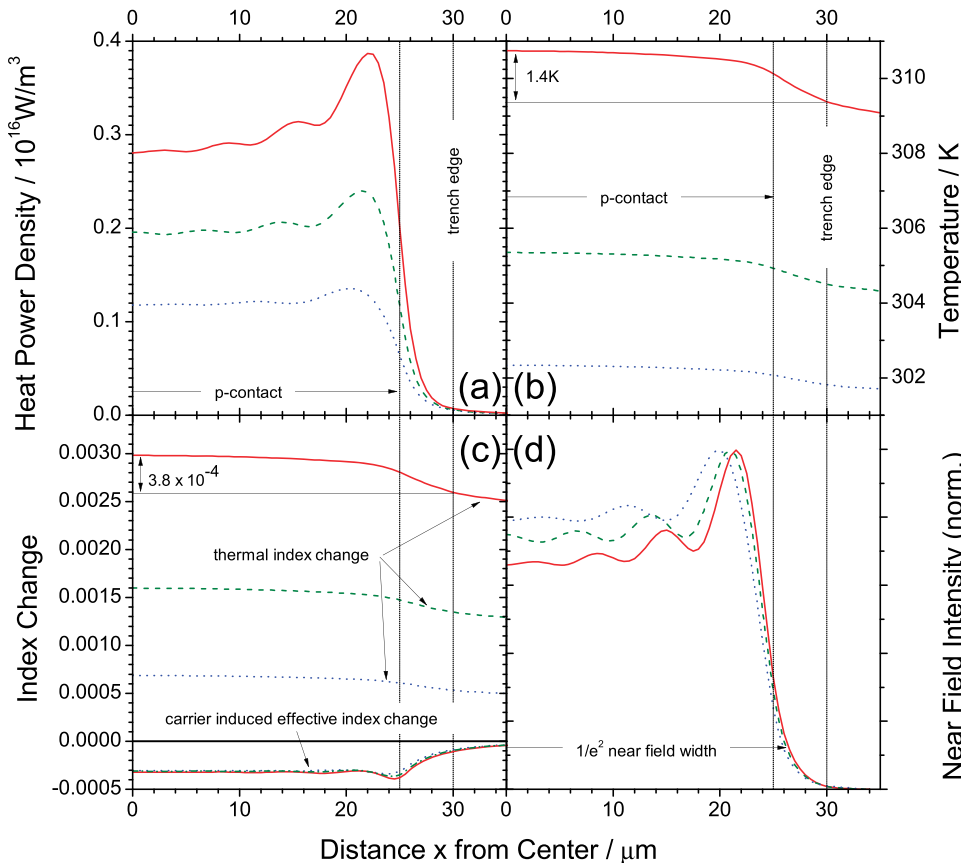


FIG. 3. Lateral profiles inside the top quantum well for half the laser diode (the left axis is the symmetry plane) at 0.6 A (dotted lines), 1 A (dashed lines), and 1.5 A (solid lines): (a) heat power density, (b) temperature, (c) refractive index change due to heating and due to carrier accumulation, (d) near field intensity.

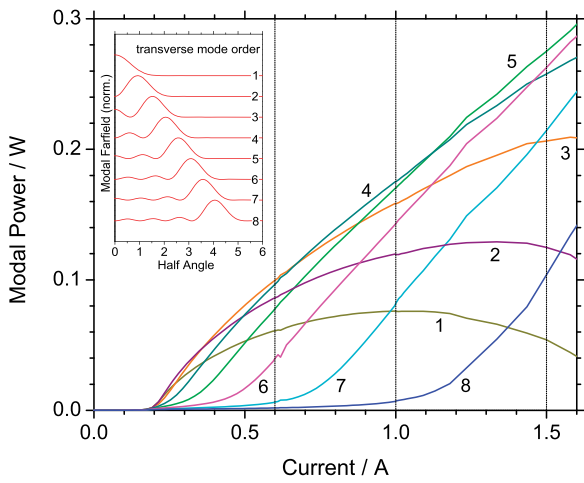


FIG. 4. Modal power vs. current (parameter: lateral mode order). The inset gives half the normalized far field profile for each lasing mode. The vertical lines mark the reference current values (0.6 A, 1 A, 1.5 A).

Figure 4 shows the simulated light-current characteristics for each lateral lasing mode. The mode order gives the number of intensity peaks. In agreement with the measurements,<sup>1</sup> each current step triggers the lasing of an additional lateral mode of higher order, which results in a wider far field (see inset of Fig. 4). At 0.6 A drive current, 6 lateral lasing modes are simulated, 7 modes at 1 A, and 8 modes at 1.5 A. The resulting total far field width is plotted in Fig. 5 and it is also in good agreement with the measurement. Thus, the far-field blooming is clearly linked to an increase in lateral mode order.

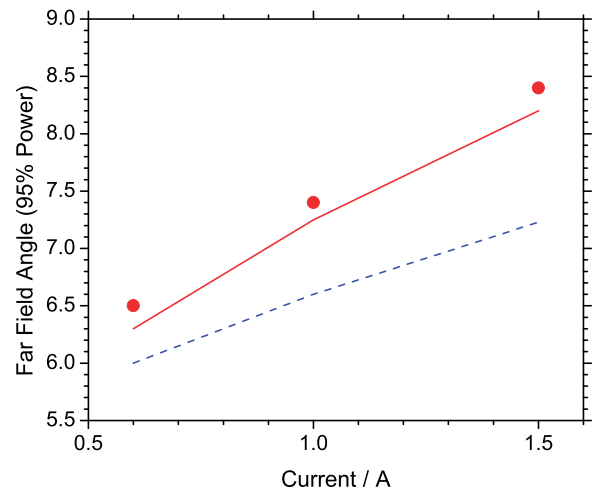


FIG. 5. Full width far field angle (95% power) vs. current as measured (symbols) and calculated (solid line). The dashed line gives the simulation result without self-heating ( $T = 298$  K).

We now investigate non-thermal blooming mechanisms by turning off the self-heating in the simulation. Surprisingly, the resulting far field still widens considerably with higher current (dashed line in Fig. 5). The physical reasons for this non-thermal far field blooming are analyzed in the following.

Figure 6 plots relevant non-thermal lateral profiles inside the top quantum well. Rising current leads to an increasing current crowding (Fig. 6(a)) which contributes to an enhanced QW carrier density near the contact edges in

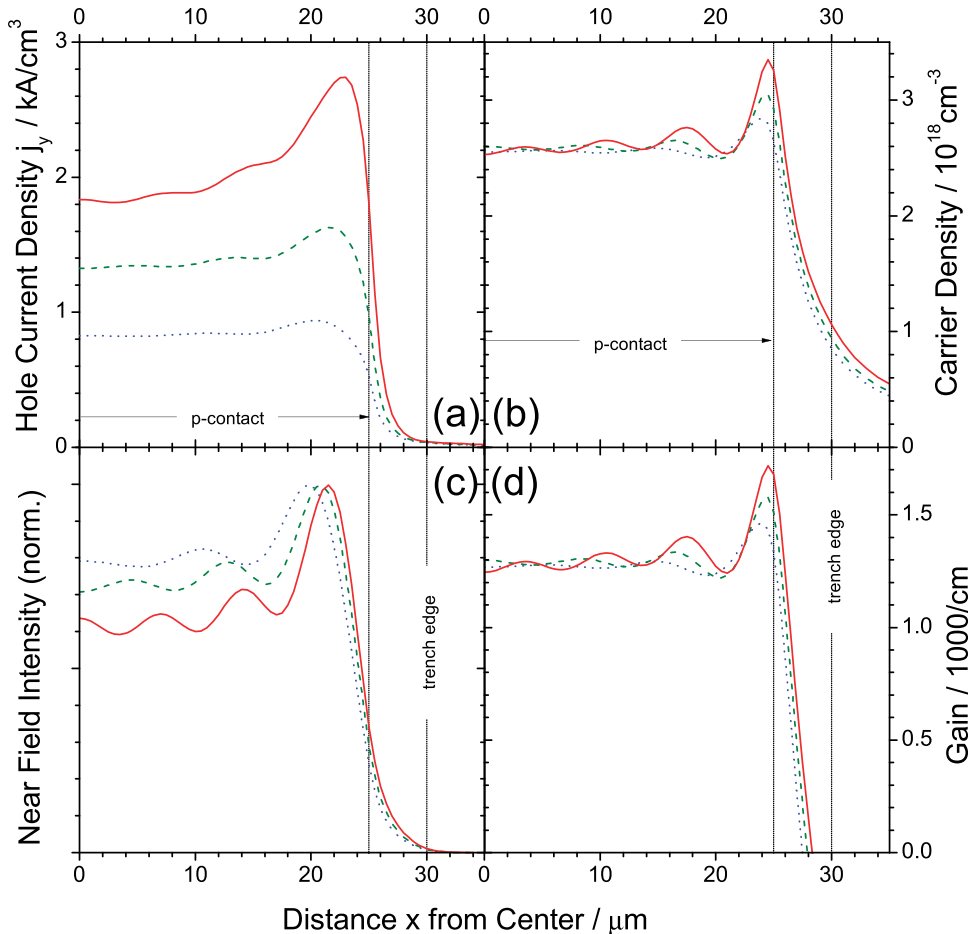


FIG. 6. Lateral profiles inside the top quantum well for half the laser diode without self-heating at 0.6 A (dotted lines), 1 A (dashed lines) and 1.5 A (solid lines): (a) vertical hole injection current density, (b) carrier density, (c) near field intensity, (d) material gain.

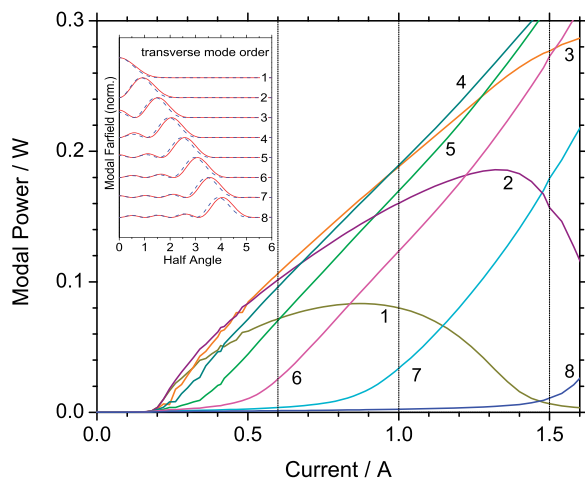


FIG. 7. Modal power vs. current without self-heating (parameter: lateral mode order). The inset gives half the normalized far field profile for each mode with (solid line) and without self-heating (dashed line). The vertical lines mark the reference current values (0.6 A, 1 A, 1.5 A).

Fig. 6(b). The resulting profile of the material gain also exhibits a pronounced peak at the contact edge (Fig. 6(d)). Both the carrier and gain profiles widen slightly with current. The gain turns into absorption at about  $x = 28 \mu\text{m}$ , only  $3 \mu\text{m}$  outside the p-contact edge. Thus, lateral carrier and gain spreading is relatively small in this laser, which is partially attributed to the contact definition by ion implantation. The resulting near field is plotted in Fig. 6(c) and its total width is about  $0.5 \mu\text{m}$  larger than with self-heating. The tail of the near field ( $x > 28 \mu\text{m}$ ) is subject to QW absorption, similar to the case with self-heating since the gain region width of  $x = 28 \mu\text{m}$  hardly changes. The effect of such optical pumping on the far field was shown to increase with higher front facet reflectivity.<sup>12</sup>

The modal light-current characteristics calculated without self-heating are shown in Fig. 7. As before, rising current triggers the onset of higher-order lateral lasing modes, but somewhat delayed compared to the self-heating case in Fig. 4. The inset of Fig. 7 shows a slight narrowing of the far field for each mode, compared to the full simulation. While eight modes contribute to the lasing process at 1.5 A in Fig. 4, the 8th mode is just at threshold in Fig. 7. At the same current, the fundamental mode disappears in Fig. 7. Such weakening of the fundamental mode with rising current was also observed in the full simulation (Fig. 4) as well as in the

measurement.<sup>1</sup> The power loss of low-order modes can be explained by the increasing gain peak near the contact edges (Fig. 6(d)) which favors higher-order modes. The non-uniform gain profile is caused in part by lateral hole burning, i.e., by QW carrier depletion due to stimulated emission (cf. Fig. 6(b)). Another part of the gain non-uniformity can be attributed to non-uniform hole injection as shown in Fig. 6(a). This hole current crowding increases significantly with rising current. Thus, the non-thermal far field blooming is mainly caused by the increasingly non-uniform distribution of carriers and gain in the quantum well, which supports high-order modes and weakens low-order modes.

These non-thermal processes are comparable to the spatial hole burning and electrical over pumping identified in earlier investigations.<sup>12,13</sup> Possible remedies are, for instance, gain tailoring<sup>14</sup> or optimized waveguide doping.<sup>12</sup>

This work was partially supported by the Ferdinand Braun Institute, Berlin, Germany.

- <sup>1</sup>P. Crump, S. Böldicke, C. M. Schultz, H. Ekhteraei, H. Wenzel, and G. Erbert, *Semicond. Sci. Technol.* **27**, 045001 (2012).
- <sup>2</sup>G. R. Hadley, J. P. Hohimer, and A. Owyong, *J. Quantum Electron.* **24**, 2138 (1988).
- <sup>3</sup>R. L. Lang, A. G. Larsson, and J. G. Cody, *J. Quantum Electron.* **27**, 312 (1991).
- <sup>4</sup>S. Blaaberg, P. M. Petersen, and B. Tromborg, *J. Quantum Electron.* **43**, 959 (2007).
- <sup>5</sup>J. Pomplun, H. Wenzel, S. Burger, L. Zschiedrich, M. Rozov, F. Schmidt, P. Crump, H. Ekhteraei, C. M. Schultz, and G. Erbert, *Proc. SPIE* **8255**, 825510 (2012).
- <sup>6</sup>See [www.crosslight.com](http://www.crosslight.com) for LASTIP by Crosslight Software Inc., Burnaby, Canada (2012).
- <sup>7</sup>J. Carroll, J. Whiteaway, and D. Plump, *Distributed Feedback Semiconductor Lasers* (SPIE Press, Bellingham, 1998).
- <sup>8</sup>J. Piprek, *Photon. Technol. Lett.* **25**, 958 (2013).
- <sup>9</sup>S. Gehrsitz, F. K. Reinhart, C. Gourgon, N. Herres, A. Vonlanthen, and H. Sigga, *J. Appl. Phys.* **87**, 7825 (2000).
- <sup>10</sup>S. Böldicke, "Characterization of lateral modes in broad-area lasers (in German)," Diploma Thesis (Technical University of Berlin, Electr. & Comp. Eng. Dept., Germany, 2010).
- <sup>11</sup>J. Piprek, *Semiconductor Optoelectronic Devices: Introduction to Physics and Simulation* (Academic Press, San Diego, 2003).
- <sup>12</sup>J. J. Lim, T. M. Benson, and E. C. Larkins, *J. Quantum Electron.* **41**, 506 (2005).
- <sup>13</sup>S. Sujecki, L. Borruel, J. Wykes, P. Moreno, B. Sumpf, P. Sewell, H. Wenzel, T. M. Benson, G. Erbert, I. Esquivias, and E. C. Larkins, *J. Sel. Top. Quantum Electron.* **9**, 823 (2003).
- <sup>14</sup>J. R. O'Callaghan, J. Houlihan, V. Voignier, G. Huyet, J. G. McInerney, B. Corbett, and P. A. O'Brien, *Photon. Technol. Lett.* **14**, 9 (2002).